Hole states in Ge/Si quantum-dot molecules produced by strain-driven self-assembly

A. I. Yakimov,[a] G. Yu. Mikhalyov, A. V. Dvurechenskii, and A. I. Nikiforov
*Rzhanov Institute of Semiconductor Physics, Siberian Branch of the Russian Academy of Sciences,
630090 Novosibirsk, Russia*

Space-charge spectroscopy was employed to study hole emission from the confined states in vertically self-aligned double Ge quantum dots separated by a Si barrier. From the temperature- and frequency-dependent measurements, the hole binding energy was determined as a function of the separation between the dots, t_{Si}. Increasing of the ground state hole energy due to formation of a bonding molecular orbital was found to be as large as $\sim$50 meV at $t_{Si}=1.5$ nm. For a dot layer separation exceeding 3 nm, the hole binding energy in double-dot molecule becomes smaller than the ionization energy of the single Ge dot, contrasting with a simplified quantum-mechanical molecular model. To analyze the experiment the electronic structure of two vertically coupled pyramidal Ge quantum dots embedded in Si was investigated by a nearest neighbor tight-binding single-particle Hamiltonian with the sp^3 basis. The elastic strain due to the lattice mismatch between Ge and Si was included into the problem. The three-dimensional spatial strain distribution was found in terms of atomic positions using a valence-force-field theory with a Keating interatomic potential. It was demonstrated that formation of single-particle hole states in self-organized molecules is governed by the interplay among two effects. The first is the quantum-mechanical coupling between the individual states of two dots constituting the molecule. The second one originates from asymmetry of the strain field distribution within the top and bottom dots due to the lack of inversion symmetry with respect to the medium plane between the dots. Analysis of the biaxial strain distribution showed that anomalous decreasing of the hole binding energy below the value of the single dot with increasing interdot separation is caused by the partial strain relaxation upon dot stacking accompanied by the strain-induced reduction of the hole confinement potential. We found that the molecule-type hole state delocalized fairly over the two dots is formed only at $t_{Si}<3.3$ nm and at $t_{Si}>3.8$ nm. For the intermediate distances (3.3 nm $\leq t_{Si} \leq$ 3.8 nm), the hole becomes confined mostly inside the bottom, most strained Ge dot. The overall agreement between theory and experiment turns out to be quite good, indicating the crucial role played by strain fields in electronic coupling of self-assembled quantum-dot molecules. © *2007 American Institute of Physics.* [DOI: 10.1063/1.2809401]

I. INTRODUCTION

Coherent two-level systems and the quantum logic gates are suggested to serve as the building blocks of a quantum information processing.[1–4] Two vertically[5,6] or laterally[7–9] coupled quantum dots (QDs) confined electrons, holes, or excitons have been proposed as a basis for entangled quantum bit operations in the solid state. Spin or charge degrees of freedom are exploited for encoding and manipulating quantum information. Apart from the obvious practical uses, "artificial molecules" are extremely interesting also from the fundamental point of view, since the relative contribution of single-particle tunneling and Coulomb interaction in them can be varied in a controllable way.[10] The electronic coupling between QDs brought closely together arises from the process of quantum-mechanical tunneling and appears as a formation of bonding and antibonding molecule-type orbitals from the single-dot states (Fig. 1) by an analogy with the covalent bonds in natural molecules. The bonding molecular state has a larger binding energy than the energies of the

original states of the individual dots, thus creating the binding force between the two dots. The collectivized electron behaves now as a coherent wave that is delocalized over both constituent QDs.

A number of transport experiments have been made with artificial molecules composed of QDs in which the lateral confinement was achieved either via etching techniques or metal gate electrodes.[7,8,11–14] However, the size of these structures is too large ($>50–100$ nm) and the interlevel spacing is too small ($\sim$1 meV) to operate a device at elevated temperatures. The phenomenon of strain-induced self-assembly of semiconductor nanostructures provides another method that allowed for the fabrication of high-quality vertically aligned QDs whose size is extremely small ($\sim$10 nm) and the electronic state resembles certainly those of an atom even at room temperature. During heteroepitaxial growth of lattice mismatched materials strain field of a dot in a first layer penetrates into the barrier material and makes it favorable for the dot on the upper layer to form above the buried QD,[15] thus forming a vertical QD molecule (QDM). Inhomogeneous spatial strain distribution is a characteristic

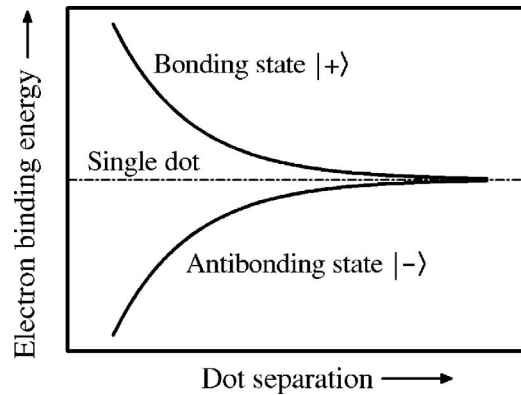a)Electronic mail: yakimov@isp.nsc.ru

FIG. 1. Schematic picture of energies of the two low-lying electron states in a QD molecule as a function of the separation between the dots. The bonding orbital $|+\rangle$ is a symmetric linear superposition of the single-dot states $|0\rangle$ and $|1\rangle$: $|+\rangle = [|0\rangle + |1\rangle]/\sqrt{2}$, while the antibonding state represents the antisymmetric wave function combination: $|-\rangle = [|0\rangle - |1\rangle]/\sqrt{2}$.

feature of self-assembled QDMs that distinguish them from electrostatically confined nanostructures. The hydrostatic component of strain usually shifts the conduction and valence band edges of semiconductor; biaxial strain, on the other hand, affects the valence bands by splitting the degeneracy of the light- and heavy-hole bands. Since the strain modifies the confinement potential and the carrier effective masses, it may cause considerable deviations from the simplified molecular behavior which implies a coupling of identical QDs.

To date, most theoretical[16–20] and experimental[6,21–27] studies on the molecular states in stacked QDs have been concentrated on self-assembled InAs/GaAs QDs. Luyken *et al.*[21] concluded that the many-body ground states of vertically aligned InAs QDs are mainly affected by interdot Coulomb coupling. Boucaud *et al.*[22] observed the terahertz (2.4 THz) absorption caused by transition between bonding and antibonding electron states in InAs/GaAs. Fonseca *et al.*[16] found that anisotropy in the strain field and associated piezoelectric potential leads to enhancing level splitting for electron molecular states. Sheng and Leburton[19] reported the anomalous quantum-confined Stark effect caused by the biaxial strain distribution in InAs/GaAs QD molecules. The resonant current with peak-to-valley ratio above 1000 was detected by Bryllert *et al.*[25] for a single InAs/InP QDM. He *et al.*[20] demonstrated that a molecule made of two identical, strained InAs/GaAs QDs exhibits asymmetry of the molecular orbitals due to inhomogeneous strain.

The Coulomb charging effect was also observed in double-layer GeSi QDs occupied with holes.[28,29] Ge quantum dots in Si(001) (4.2% lattice mismatch) is another system exhibiting a self-organization of nanostructures in semiconductor heteroepitaxy.[30] The large (~ 0.7 eV) valence band offset of Ge/Si(001) heterojunction leads to effective localization of holes in the Ge islands, whereas the electrons are free in the Si conduction band.[31] Usually, the behavior of holes in low-dimensional systems is more complicated than that of electrons because of the complex valence band structure in III-V and IV semiconductors. The hole state in Ge QD is built mainly from valence-band states, namely, heavy-

hole states $|\frac{3}{2}, \pm\frac{3}{2}\rangle$, the light-hole states $|\frac{3}{2}, \pm\frac{1}{2}\rangle$, and the split-off hole states $|\frac{1}{2}, \pm\frac{1}{2}\rangle$. Here, $|J, J_z\rangle$ are the eigenstates of the effective angular momentum J and its projection J_z. The strong mixing between the light- and heavy-hole states is a result of the uncertainty in all components of quasi-impulse owing to hole spatial confinement both in vertical and lateral directions.[32] In uniaxially strained semiconductors, strains lifts the degeneracy of the valence band, making the heavy hole states to be the highest valence band.[33] For this reason, the contribution of the heavy hole states in the ground state of QDs must be predominant. As demonstrated by tight-binding calculations,[34] in Ge nanoclusters with lateral size of ~ 15 nm and height of ~ 1.5 nm, the contribution of the state with $J_z = \pm\frac{3}{2}$ is about 90%. Because the strain extends into the barrier material, the strain field within one QD is affected by a neighboring dot as well. One can expect that redistribution of strain fields during vertical stacking of Ge dots would substantially modify the band structure which, in turn, will strongly affect the formation of molecular orbitals.

In this paper we analyzed both experimentally and theoretically the single-particle hole ground state of double Ge/Si quantum dot representing an ionized "artificial hydrogen molecule" containing a hole instead of an electron. We observed that the ground-state configuration undergoes nontrivial transformations as a function of the interdot distance due to the competition of the tunneling and deformation effects.

II. EXPERIMENTAL DETAILS

Samples were grown by molecular-beam epitaxy on a p^+–Si(001) substrate with a resistivity of 0.005 Ω cm doped with boron up to a concentration of $\sim 10^{19}$ cm^{-3}. After preliminary chemical processing, the substrates were placed in the growth chamber where they were cleaned by a weak Si flux at 800 °C for 15 min. As a result of cleaning, an atomically pure surface with a sharp (2×1) diffraction pattern is formed. The growth temperature was 500 °C for all layers. The active region consists of two nominally pure Ge layers separated by Si spacer layer of thickness t_{Si} [Fig. 2(a)]. Immediately after the deposition of Ge, the temperature was lowered to $T_s = 350 - 400$ °C and the Ge islands are covered by a 1 nm Si layer. This procedure is necessary to minimize Ge–Si intermixing and to preserve island shape and size from the effect of a further higher temperature deposition.[35–38] In order to reduce distortion of the hole confining potential by the potential of ionized impurities, 10 nm thick undoped Si spacers were introduced between the topmost (bottom) Ge layer and the p-type Si cover (buffer) layer. The boron concentration in the 0.35 μm thick cap and 0.5 μm thick buffer Si layers was $\sim 4 \times 10^{16}$ cm^{-3}. To identify effects of dot coupling, the reference sample was grown under conditions similar to the QDM samples, except that only a single Ge layer was deposited.

The Ge QD formation was controlled by reflection high energy electron diffraction when the pattern changed from streaky to spotty. The transition from two-dimensional to three-dimensional island growth was observed after ~ 4 monolayers (1 ML=1.41 Å) of Ge deposition both for the
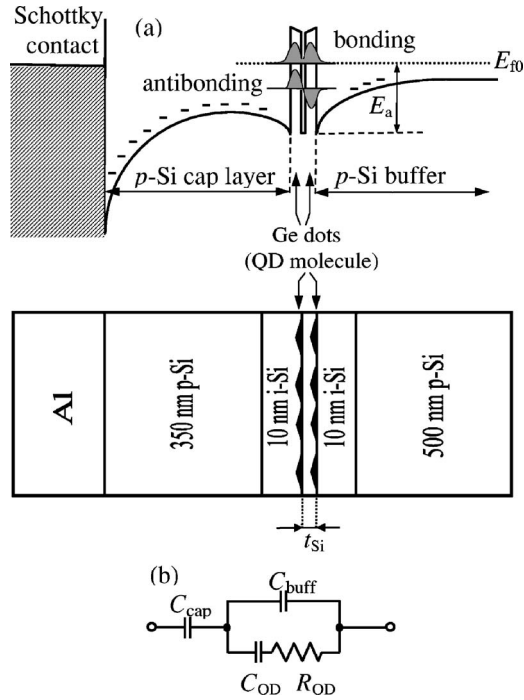
FIG. 2. (a) A schematic valence band diagram of the Si Schottky diode containing a double stack of Ge QDs and a sketch of the sample structure. The p^+-Si substrate is not shown. (b) Equivalent electrical circuit for the ac response from the dots lying inside the depletion region. C_{cap} is the capacitance of the totally depleted capping Si layer, C_{buff} the capacitance of the depleted portion of the buffer Si layer, C_{QD} the QD capacitance, and R_{QD} the hole emission and capture resistance.
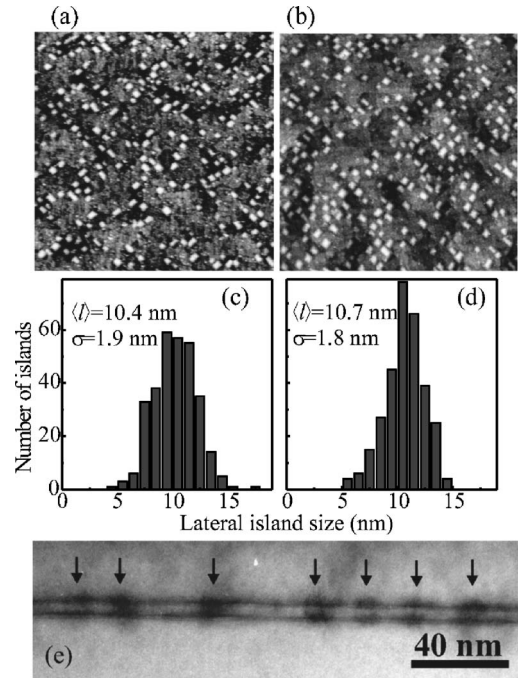

FIG. 3. 400×400 nm^2 STM images [(a) and (b)] and size distribution histograms [(c) and (d)] from topmost uncapped Ge layer of single [(a) and (c)] and double [(b) and (d)] island layers deposited at a substrate temperature of 500 °C with the rate of $R=1$ ML/s. For the twofold stack in panels (b) and (d), the separation between Ge layers is 3 nm. Image sides are oriented along the [110] crystalline directions. (e) Cross-section TEM image in (001) direction of coupled Ge QDs separated by a Si barrier with 3.5 nm thickness. Arrows indicate vertically coupled double quantum dots.

first and second Ge layers. The Ge growth rate was chosen to be as large as $R=1$ ML/s to provide the high Ge content in the islands.[39] The average Ge content of 80%–90% (depending on t_{Si}) in the nanoclusters was determined from Raman measurements. The scanning tunneling microscopy (STM) of samples without the Si cap layer was employed to assess the morphology of Ge layers. Figures 3(a) and 3(b) show the STM images of the topmost Ge layer for single and double-layer samples, and the lateral size histogram derived derived for each image. In good qualitative agreement with the results obtained previously in Refs. 40 and 41, the surface morphology is approximately the same for the single and double island layers, and changes significantly with further increasing of the number of Ge layers in the structure. Although, some of the islands did not have a square base, we used their geometrical mean, $l=\sqrt{l_\parallel \times l_\perp}$ ($l_\parallel$ and $l_\perp$ are the island base lengths), as a convenient measure of their size. From these data, the width of the size distribution, σ, was calculated as standard deviation,

$$\sigma^2 = \frac{1}{n-1}\sum_{i=1}^{n}(l_i - \langle l \rangle)^2,$$

where n is the number of islands evaluated, and $\langle l \rangle$ is the mean size. Ge nanoclusters have a shape of "hut" clusters bounded by {105} facets[42] with predominantly square bases in two orthogonal orientations, corresponding to $\langle 100 \rangle$ directions in the substrates. The dots have a typical base length $\langle l \rangle \simeq 10-11$ nm and an areal density $n_{QD}=1.5 \times 10^{11}$ cm^{-2}. The nonuniformity of island size is estimated to be about

16%–18%. Figure 3(e) shows a representative cross-sectional transmission electron micrograph (TEM) of a double-layer sample with $t_{Si}=3.5$ nm. The image clearly demonstrates the formation of double-dot molecules with a high vertical correlation between Ge islands.

For the capacitance and conductance measurements, Al contacts were deposited on top of the samples through a shadow mask to form a Schottky diode, while the Ohmic back contact was fabricated by alloying indium to the p^+-type Si substrate. The area of the Al contacts was $A=8 \times 10^{-3}$ cm^2. Just before the metallization, a 30 nm top Si layer was etched off to remove any remaining contamination from the surface. The admittance was measured using a Fluke PM6306 *RLC* meter in the frequency range from 100 Hz to 1 MHz. The amplitude of the ac modulation voltage was 50 mV. At each frequency, the *RLC* meter was carefully calibrated to compensate for the parasitic resistance from the measurement circuit. A Keithley 6430 subfemtoampere remote source meter was used for supplying a dc bias voltage. Both meters were controlled by the computer system through the IEEE-488 interfaces.

III. DATA ANALYSIS PROCEDURE

A. Determination of the hole binding energies

To determine the hole binding energy we measured the hole thermal emission rates at different temperatures using admittance spectroscopy. In these experiments, the ac conductance G of a *pn* junction or Schottky diode with the elec-

tronic states of interest is measured as a function of temperature for a fixed reverse bias U_b and test frequency $\omega = 2\pi f$. For a given measurement frequency, the conductance reaches a maximum at a temperature T_{max} which corresponds to the condition[43]

$$\omega \approx 2 e_p (T_{max}), \tag{1}$$

where

$$e_p(T) = B\sigma_p T^2 \exp(-E_a/k_B T) \tag{2}$$

is the emission rate of electrons or holes from the bound to extended states, $B = 16\pi m^* k_B^2 / g_t h^3$ is a temperature independent factor, m^* is the effective mass of the density of states, g_t is the degeneracy of a quantum level, h is the Plank's constant, σ_p is the capture cross section, k_B is the Boltzmann constant, and E_a is the activation energy being determined by the actual path whereby holes escape from the dots to the Si valence band. By measuring the $G(T)$ dependencies at various ω, the activation energies of hole emission rate and the capture cross section σ_p can be deduced from the Arrhenius plot of $e_p(T_{max})/T_{max}^2$ vs $1/T_{max}$. With changing of the reverse bias U_b, the chemical potential scans through the density of hole states in the QD layer [Fig. 2(a)]. At higher reverse bias, the chemical potential crosses deeper states in the dots. Thus, from the bias-variable temperature- and frequency-dependent measurements the energy of hole emission from different confined states can be determined.

B. Effect of electric field on the hole thermal emission

In a simple scenario of emission by thermal excitation from the localized states in the QD layer to the continuum, E_a corresponds to the binding energy of holes with energies close to the Fermi level. In more complex cases E_a may deviate from this energy. The electron escape process in InAs/GaAs QDs is known to be a two-step process[43–48] which involves thermal activation to the excited state where the tunnel probability is more favorable and then subsequent tunneling into the GaAs conduction or valence band by the assistance of electric field. Therefore, both the localization energy and the electric field are important for the electron emission from QDs with a small carrier effective mass. In Ge/Si QDs, hole tunneling should be vastly suppressed for due to the large hole effective mass in Si ($m_h^* = 0.49 m_0$) and the large localization energy (300–400 meV),[49–54] thus making the hole emission to be purely thermally activated. As described by Chang *et al.*[44] and Geller *et al.*,[48] the apparent capture cross section σ_p is expected to grow in electric field due to increasing transparency of a triangle tunneling barrier. Instead, we observed the opposite behavior (see, Fig. 9) that signals against the importance of field-assisted tunneling process in our samples.

To obtain further support for this statement, we estimated the possible effect of electric field on the hole emission rate. The estimation is based on the model of Vincent *et al.*[55] who considered phonon-assisted tunneling between a Dirac well and an energy band. The ratio of the thermal emission rate with or without electric field is represented by[55]

$$\frac{e_p(F)}{e_p(0)} = 1 + \int_0^{E_a(0)/k_B T} \exp\left[z - z^{3/2} \left(\frac{4}{3} \frac{(2m_h^*)^{1/2} k_B T^{3/2}}{q\hbar F} \right) \right] dz, \tag{3}$$

where $E_a(0)$ is the hole binding energy in zero field, and F is the electric field strength. The field-assisted tunneling becomes important when

$$T \ll T_c = \frac{(q\hbar F)^{2/3}}{k_B (8m_h^*)^{1/3}}. \tag{4}$$

We calculated the mean electric field across the dots on the basis of the quasistatic charging model and self-consistent calculations of Poisson equation described in Ref. 54. At the onset of dot charging with holes, $F \approx 3 \times 10^6$ V/m. In this way, we find $T_c = 60$ K, while all measurements in this work were performed at $T > 150$ K.

The phenomenon of field-assisted tunneling via the wetting layer in Ge dots may take place when the number of confined holes in each Ge island is large enough ($\geqslant 10$) producing a strong electric field around the islands,[56] which is not the case for the samples under investigation. Thus, effect of the two-step escape on the hole emission energy in Ge/Si QDs may not be taken into account in the present study.

A further possible manifestation of the electric field is a lowering of the emission barrier by the field F due to the Poole-Frenkel effect.[45,47,57] Assuming a square-well confinement in field direction the true emission energy differs from the measured activation energy by $\Delta U = qFh/2$, where h is the QD height. We find that, for the bias applied here, ΔU is less than 3 mV implying that the barrier lowering effect also play a minor role in our samples.

C. Determination of the average dot filling factor

For a given QDM density n_{QD} one may introduce the average number of extra holes per each molecule ν, which by analogy with quantum Hall effect can be called the filling factor. The average molecule filling factor is controlled by the gate voltage U_b and defined by

$$\nu(U_b) = p_{QD}(U_b)/n_{QD}, \tag{5}$$

where $p_{QD}(U_b)$ is the hole density in the dot layer (here, we assume that the dot density in the single-layer sample is equal to the density of "diatomic" molecules in the double-layer samples). Usually the charge density is derived using C-V profiling procedure. However, for the case of a heterojunction, the measured apparent carrier concentration differs from the true local carrier concentration due to Debye length smearing.[58] Therefore, we used another approach. The equilibrium density of holes accumulated in QDs was extracted from the capacitance of the dot or molecule layer using the equation

$$p_{QD}(U_b) = \frac{1}{qA} \int_{u_0}^{u} C_{QD}(u) du, \tag{6}$$

where C_{QD} is the quantum-dot-layer capacitance, u is the the electrostatic potential at the position of the dot layer caused by dot charging at the applied bias U_b, u_0 corresponds to a
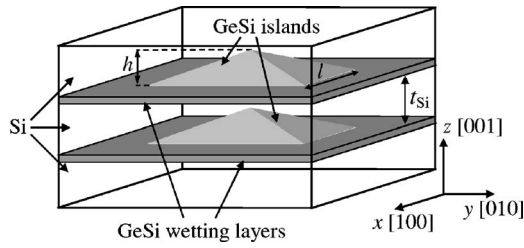
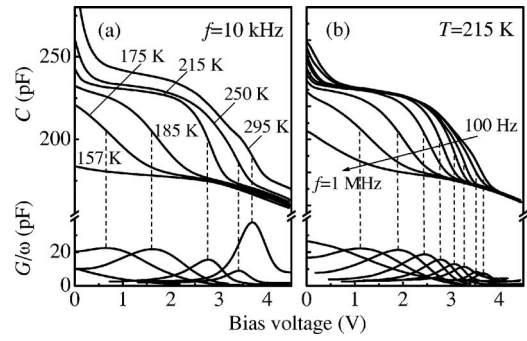FIG. 4. Schematic picture of a Ge/Si QD molecule used for a simulation of molecular states.

FIG. 5. (a) Temperature dependence of the capacitance-voltage and conductance-voltage characteristics measured at $f=10$ kHz. (b) *C-V* and *G-V* characteristics measured at $T=215$ K and modulation frequencies 0.1, 0.3, 1, 3, 10, 30, 100, 300, and 1000 kHz. The sample contains two layer of Ge QDs separated by a 2 nm Si spacer.

bias at which all holes escape from QDs and $C_{QD}(u_0)=0$. The value of u_0 can be determined from known doping level by a procedure described in Ref. 59.

In order to evaluate the QD capacitance it is necessary to construct the equivalent electrical circuit which reproduces the ac response from the dots. For simplicity we consider only biases for which the depletion width of the metal-semiconductor (Al–Si) junction extends to the QD layer. In our samples, capacitance-voltage measurements (Sec. IV A) demonstrate that QDs lie inside the depletion region just at $U_b > 0-1$ V depending on the sample. From Anand *et al.*,[57] an ac response from the dots can be treated as a lossy capacitor of time constant $\tau = R_{QD}C_{QD}$. In this case the equivalent circuit consists of the depletion capacitance of the Si cap layer C_{cap} in series with a parallel combination of the capacitance of the depleted part of the Si buffer layer C_{buff} and series *RC* network with the quantum-dot capacitance C_{QD} and time constant τ [Fig. 2(b)]. The cap layer capacitance C_{cap} is easily calculated with known values of device area A and the cap layer thickness L. C_{cap} is assumed to be independent of U_b, ω, and T and equals to $C_{cap} = \epsilon\epsilon_0 A/L$, where ϵ and ϵ_0 are the relative and absolute permittivities, respectively.

Now the relationship between u and gate voltage U_b can be determined from[60]

$$u(U_b) - u_0 = -\int_{U_{b0}}^{U_b}\left[1 - \frac{C_0(U_b')}{C_{cap}}\right]dU_b', \qquad (7)$$

where U_{b0} is the reverse bias at which QDs are neutral, C_0 is the sample capacitance in the low-frequency limit ($\omega\tau \ll 1$). The capacitance contribution given by the holes in QDs is deduced from the frequency-dependent *C-V* measurements,

$$C_{QD}(U_b) = \left(\frac{1}{C_0(U_b)} - \frac{1}{C_{cap}}\right)^{-1} - \left(\frac{1}{C_\infty(U_b)} - \frac{1}{C_{cap}}\right)^{-1}, \qquad (8)$$

where $C_\infty(U_b)$ is the high-frequency device capacitance. Analysis of the experimental *C-V* characteristics by using Eqs. (5)–(8) allows one to calibrate the relationship between the average dot filling factor and the gate voltage.[61]

D. Hole states treated with tight-binding approach

For a simulation, we considered two *identical* vertically aligned pyramidal GeSi islands with four {105}-oriented facets and a (001) base embedded into the Si matrix, as shown in Fig. 4. Each pyramid lies on a 4 ML Ge$_{0.9}$Si$_{0.1}$ wetting

layer and contains 10% Si atoms randomly distributed within QD. About 17–20 realizations of Si atoms distribution were analyzed. The final results were obtained by averaging over these realizations. The islands are separated by a Si barrier of thickness t_{Si} measured from wetting layer to wetting layer. For simplicity, we ignored the possible dependence of the island composition on t_{Si}. The pyramid aspect ratio h/l is fixed and equals to 0.1. The typical size of computational cell (GeSi wetting layers plus GeSi islands plus Si environment) is $30a \times 30a \times 24a$ along the x, y, and z axes, respectively, where $a = 5.431$ Å is the Si lattice constant. In order to check whether the calculation volume is large enough to give the proper (size-independent) result we performed numerical analysis also for different vertical sizes of computational domains ranging from $18a$ to $27a$ and found that the hole binding energy does not depends on the size of supercell to within 1 meV of accuracy.

The strain distribution was found in terms of atomic positions, using valence-force-field (VFF) model with a Keating interatomic potential,[62,63] previously adopted for single self-assembled InAs/GaAs and Ge/Si QDs with different shapes, sizes, and composition,[34,64–71] and for multilayer Ge/Si structures.[72,73] In comparison with the finite-difference[74] and finite-element methods,[75–78] which are also often used for the strain calculations of QDs, the advantage of the VFF model is that the strain energies and the positions of all the atoms in a supercell can be obtained.

We considered the ground state of a double dot occupied with only one hole. Thus, the system under study represents an ionized "artificial hydrogen molecule." The eigenvalue problem for the hole ground state in QD molecule was solved with the sp^3 tight-binding (TB) approach, including interactions between nearest neighbours only.[34,79,80] Following the work of Chadi,[81] spin-orbit interactions were added to the Hamiltonian. Finding eigenvalues of the Hamiltonian is performed by a method analogous to that of Pedersen and Chang.[82]

IV. EXPERIMENTAL RESULTS

A. Admittance-voltage measurements

Figure 5(a) shows the temperature evolution of the *C-V* and *G-V* characteristics of a double-layer sample with t_{Si}

=2 nm for a test frequency of f=10 kHz. Similar graphs
were also obtained for the other samples. At $U_b \gtrsim 0.5$ V, the
measured capacitance is smaller than the depletion capaci-
tance of the Si cap layer C_{cap}=250 pF. This means that the
total depletion width exceeds the cap Si layer thickness L_{cap}
and the depletion region of the metal-semiconductor junction
does really extends beyond the QD layer. Thus, the equiva-
lent circuit model displayed in Fig. 2(b) is relevant for the
data analysis procedure. At high temperature, there is a well-
pronounced capacitance plateau from 0.5 to 3.6 V associated
with the positive charge accumulation in the dot layers.[83] The
width of a plateau depends on the steady-state occupation of
hole levels in the dots. Due to the p-type doping in the Si
matrix, the Ge QDs are charged by holes at a zero bias.
When a reverse bias is applied to the diode, the holes are
gradually swept from the shallower QD states to the deeper
states. At $U_b \gtrsim 3.6$ V, all holes escape from the QDs and the
QD contribution to the measured capacitance disappears. The
corresponding step in the capacitance is accompanied by the
peak in the measured parallel conductance at voltage U_p near
the edge of the capacitance plateau. The emergence of a con-
ductance peak can be regarded as a fingerprint of a resonant
condition for charging/discharging the QDs, which is $\omega\tau$=1.
The characteristic time τ for hole exchange between the dots
and the barrier depends on both the QD confined energies
and the temperature. At low temperatures, holes freeze onto
deep states in the dots and do not participate in the ac re-
sponse. Therefore, as the temperature is reduced, the capaci-
tance plateau is suppressed and the conductance peak shifts
towards lower biases, at which the applied ac frequency reso-
nates with emission rate from shallower QD states.

Similarly, the resonant condition should be fulfilled at a
lower bias for a higher frequency. Figure 5(b) shows the C-V
and G-V characteristics recorded at T=215 K for different
test frequencies. A clear shift of the capacitance step and the
conductance maximum towards lower biases is seen as the
frequency is increased. This is consistent with the arguments
outlined above. We considered capacitance-voltage traces
taken at f=100 Hz and 1 MHz as the steady-state (low-
frequency) and the high-frequency characteristics, respec-
tively, for the calculation of the QDM filling factor ν (Sec.
III C). Bias dependence of the density of holes accumulated
on deep levels of dots and possible defects, determined as
described in Sec. III C, is shown in Fig. 6.

B. Temperature dependence of admittance

The typical temperature dependencies for the normalized
conductance measured at different modulation frequencies
and bias voltages are displayed in Fig. 7. The behavior of
$G(T)/\omega$ can be qualitatively explained as follows. At a fixed
bias, the charging/discharging process corresponds to the QD
hole level coinciding with the Fermi level in undepleted part
of the p-Si buffer layer. The rate of hole emission from this
level becomes more slow when the temperature is reduced;
therefore, with a decrease in the modulation frequency, the
condition for the conductance maximum (1) is satisfied at
lower temperatures [Fig. 7(a)]. With an increase in reverse
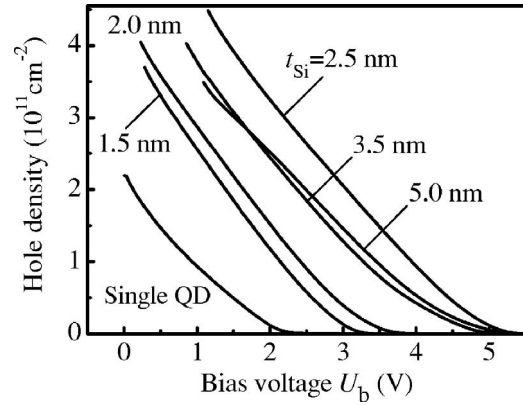bias, the holes localized at deeper QD levels, for which con-

FIG. 6. Density of holes accumulated on deep localized states as a function
of the reverse bias. The data were obtained from the low- and high-
frequency capacitance-voltage characteristics as described in Sec. III C.

dition (1) at a fixed frequency is satisfied at higher tempera-
tures, contribute to the admittance signal. For this reason, the
conductance peak in Fig. 7(b) shifts towards higher tempera-
tures with increasing U_b. At $U_b > 3.4$ V, Ge QDs become
completely depleted and the maximum on the $G(T)/\omega$ curves
disappears. This is consistent with the observation from the
C-V measurements of the same sample.

Figure 8 shows the representative dependencies
$e_p/T^2_{max}(T^{-1}_{max})$ obtained using Eq. (1) from the temperature
variation of conductance under different modulation frequen-
cies. The activation energy E_a of the hole emission rate was
found from the slope of the approximating straight lines, and
the capture cross section was determined from the point of
intersection of the approximating lines and the ordinate axis.
The linear correlation coefficients of all the lines are larger
than 0.9997 ensuring the good accuracy of the data deduced
from the plots. The capture cross section σ_p has the value of
about 10^{-13} cm^2 (Fig. 9), typical for self-assembled
QDs,[46,48,84,85] and decreases at large reverse bias due partici-
pating of deep defect traps in the capture process (see be-
low).

The resulting activation energies of the hole emission
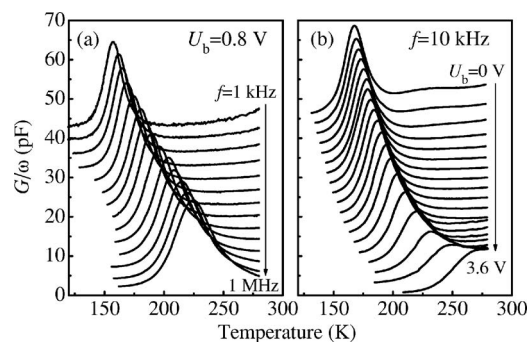rate of a series of samples with twofold stacks of Ge islands

FIG. 7. (a) Temperature dependence of the normalized conductance G/ω
recorded at U_b=0.8 V and modulation frequencies 1, 2, 3, 5, 10, 20, 30, 50,
100, 200, 300, 500, 700, and 1000 kHz. (b) Temperature dependence of the
conductance measured at modulation frequency f=10 kHz under different
bias voltages. The reverse bias is increased from U_b=0–3.6 V with an in-
crement of 0.2 V. Each conductance curve has been offset by 3 pF in panel
(a) and by 2.5 pF in panel (b) for clarity. The sample contains two layer of
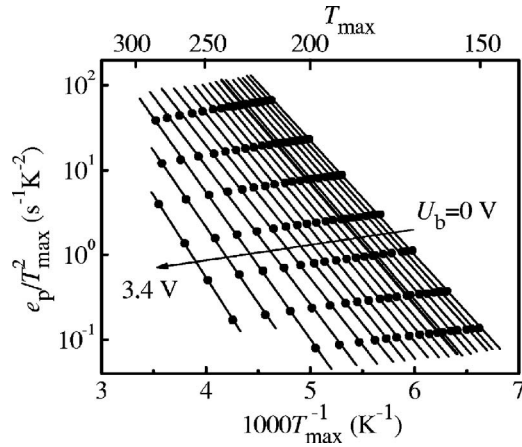Ge QDs separated by a 2 nm Si spacer.

FIG. 8. The Arrhenius plots of the hole emission rate obtained from G/ω-T traces of a double-layer sample ($t_{Si}=2$ nm) with different bias voltages. The reverse bias is increased from $U_b=0-3.4$ V with an increment of 0.2 V.

are presented in Fig. 10 as a function of U_b/U_p ratio, where U_p is the bias voltage at which the conductance peak appears in the low-frequency conductance-voltage characteristics. In our experimental conditions, U_p varies from 2.1 to 5.5 V for different samples. Near the edge of capacitance plateau (i.e., at $U_b/U_p \approx 1$), the activation energy turns out to be the same for all samples. Its value, ≈ 0.38 eV, is much larger than the ground state hole energy in the dots (see Sec. V). The corresponding hole traps are visible as an additional concentration peak at a depth of ≈ 0.4 μm in the bulk carrier concentration profiles deduced from the low-frequency capacitance-voltage characteristics (Fig. 11). The 0.38 eV level in boron-doped Si is plausibly attributed to oxygen-carbon defect complexes,[86] and is often observed as a sharp photoluminescence line at about 0.76 eV in many experiments on SiGe heterostructures.[87] An exact identification of the origin of this trap would need further investigation and is beyond the scope of this study. By integrating the defect-related peak of the concentration profiles over the depth we found the defect density to be $(8\pm1)\times10^{10}$ cm^{-2} in the samples under investigation. This number was subtracted from the total equilibrium density of trapped holes when we determined the QDM filling factor from the C-V measurements.

The final dependence of the hole emission energies on the QDM filling factor is presented in Fig. 12. The unexpected result, contrasting with a simplified quantum-
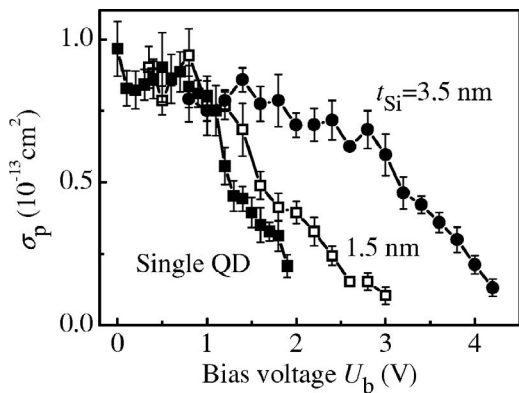
mechanical molecular model shown in Fig. 1, is that for a dot layer separation exceeding 2.5 nm, and at $\nu > 0.3$ the hole energy of the coupled dot system becomes smaller than the energy of holes in the single dot. It is commonly accepted that dispersion of the QD size is a dominating force for inhomogeneous broadening of density of states (DOS) in ensembles of QDs produced by strain-driven self-assembly. For the ground-state energy levels, DOS has a maximum at energy which corresponds to the typical dot size. On the other hand, in arrays of quantum dots, DOS oscillates as a function of filling factor and is peaked at half integer ν.[88] Therefore, to analyze the ground state of molecules occupied with only one hole, we consider the experimental data taken at $\nu=0.5$ (Fig. 13). One can see that increasing of the ground state
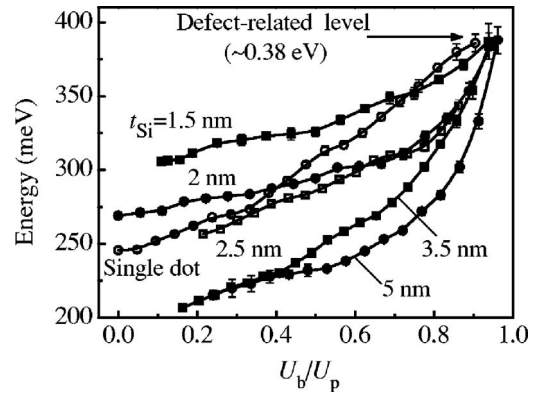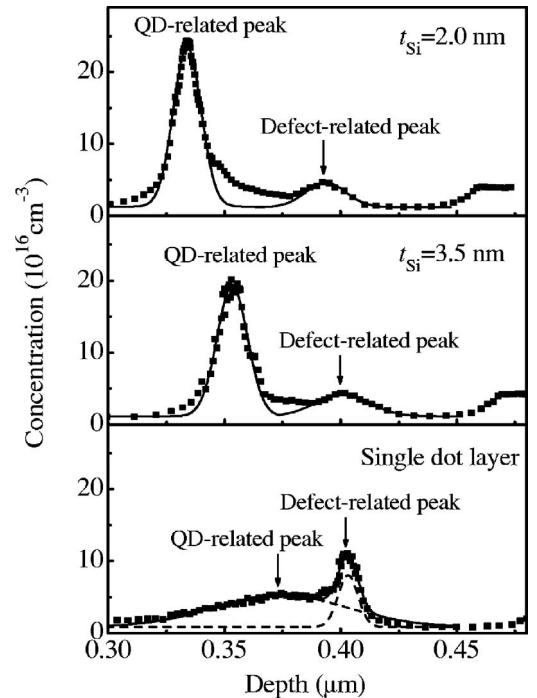

FIG. 10. Bias dependent activation energies of the hole emission rate for a series of samples where the Si spacer thickness t_{Si} was systematically varied. The E_a vs U_b dependence for a reference sample incorporating only one Ge layer is also included. The reverse bias voltage U_b is measured in units of U_p, where U_p is the voltage at which the conductance peak appears in the low-frequency conductance-voltage characteristics. Physically, U_p corresponds to onset of charging of deep traps.

FIG. 9. The capture cross section σ_p as a function of reverse bias.

FIG. 11. The typical apparent hole distribution derived from the measured C-V curves using the full depletion approximation (Ref. 60).
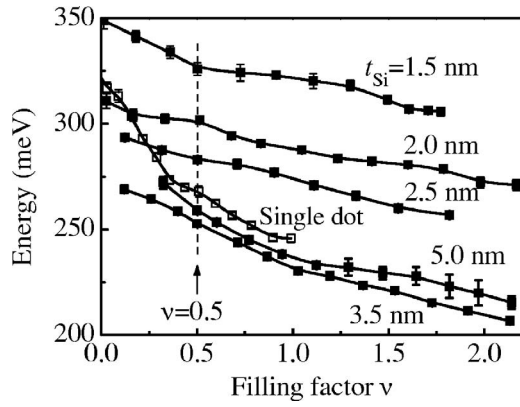
FIG. 12. Activation energies of the hole emission rate as a function of filling factor for a series of samples where the Si spacer thickness t_{Si} was systematically varied.

hole energy due to formation of a bonding molecular orbital is as large as ~50 meV at $t_{Si}=1.5$ nm. For $t_{Si}=3.5$ and 5 nm the hole binding energy is obviously smaller that the ionization energy of single dot.

It is necessary to note that for double-dot structures fluctuations of interdot separation appears to be another factor which can smear the data deduced from the experiment. To reduce effect of these fluctuations on the measured hole binding energy one has to consider the admittance data taken at applied bias for which the Fermi level lies at the maximum of the hole density of states. Since the admittance amplitude is proportional to the number of holes being exchanged between localized and extended states,[43] just in this case one probes the energy levels of dots with both typical size and interdot separation, and the impact to the capacitance and conductance signals from the dots with anomalously large and small Si spacer layers should be small. Clearly, such reverse bias corresponds to the half-integer dot filling factor, as we consider above. Therefore, we are sure that the experimental data make sense.

V. THEORETICAL RESULTS AND DISCUSSION

The interpretation of experimental results is based on the application of sp^3 tight-binding approach in combination
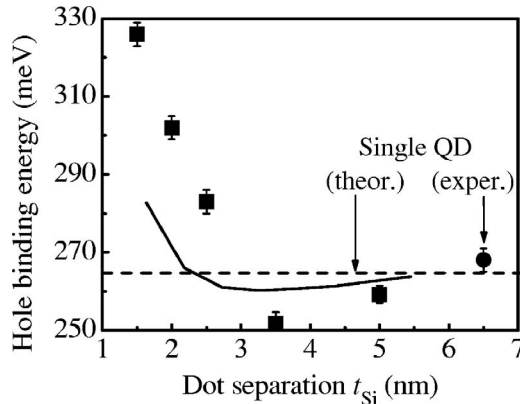

FIG. 13. Evolution of the hole emission/binding energy for $\nu=0.5$ as a function of the distance between QD layers. As reference, also the energy of single dot is shown. Circle and squares denote experimental data for single- and double-layer structures, respectively. The solid line is the result of theoretical modeling of double-dot molecules. The dashed line corresponds to the single dot.

with the valence-force-field model (Sec. III D). The solid and dashed lines in Fig. 13 represent the calculated single-particle energies with no fitting parameters have been used. The agreement between the measured and calculated values is generally good. Both the model and experiment find (i) the same hole binding energies for the single dot (~265 meV), and (ii) the reduction of the energy of a hole in coupled dots below the energy of the single dot at $t_{Si}>3$ nm. The latter effect can be considered as *anomalous* as it cannot be inferred from a simple superposition of the electronic properties of single dots. To understand qualitatively the anomalous behavior let us analyze the strain-induced shift of the heavy-hole band in bulk Ge (ΔE_{hh}) which provides the dominant contribution (~85%) to the ground hole state in Ge QDs.[34] The model-solid theory predicts[89]

$$\Delta E_{hh} = \Delta E_{hyd} + \Delta E_b, \tag{9}$$

where

$$\Delta E_{hyd} = a_v(\varepsilon_{xx} + \varepsilon_{yy} + \varepsilon_{zz}) \tag{10}$$

and

$$\Delta E_b = -b[\varepsilon_{zz} - 0.5(\varepsilon_{xx} + \varepsilon_{yy})] \tag{11}$$

are the energy shifts caused by the hydrostatic and biaxial strain components, respectively, ε_{zz}, ε_{xx}, and ε_{yy} are the diagonal components of the strain tensor, a_v and b are the respective deformation potentials. Values of the hydrostatic deformation potential a_v and the shear deformation potential b for Si and Ge can be found in Ref. 90 (note that b is negative). It is important to note that in those regions of the structure where the biaxial strain $\varepsilon_b = \varepsilon_{zz} - 0.5(\varepsilon_{xx} + \varepsilon_{yy})$ is negative, the heavy-hole band will be shifted downwards; in the regions of the positive ε_b, the heavy-hole band will be uppermost. This means that the hole confining potential formed by the valence band offset at the Ge/Si interface is reduced when the strain is relaxed inside Ge nanoclusters.

From our calculations we observed that the hydrostatic strain $Tr[\varepsilon(\mathbf{r})] = \varepsilon_{xx} + \varepsilon_{yy} + \varepsilon_{zz}$ resides entirely inside the dots and is approximately the same for the stacked structures and the single dot [Fig. 14(a)]. Unlike the hydrostatic component, the biaxial strain inside QDs is decreased when the two dots are brought closely together [Fig. 14(b)], leading to hole levels with smaller localization energies due to reduction of the hole confinement potential in the coupled dot system [see Eqs. (9)–(11)]. Thus, the observed decreasing of the hole binding energy below the value of the single dot is caused by the partial strain relaxation upon dot stacking accompanied by the strain-induced reduction of the hole confinement potential.

The hole localization in the double dots and single dot is illustrated in Fig. 15 where we plot the probability density of the ground hole state across the *y*-*z* plane. We observed that for all t_{Si} the bonding state is composed of the *s*-like individual orbitals of the top and bottom dot. At the small ($t_{Si}<3.3$ nm) and large ($t_{Si}>3.8$ nm) interdot separation, the probability to find the hole in the top or the bottom dot are comparable, suggesting a molecular-type delocalized state. However, at intermediate dot separation, the ground hole state becomes mostly localized in the bottom dot. The reason
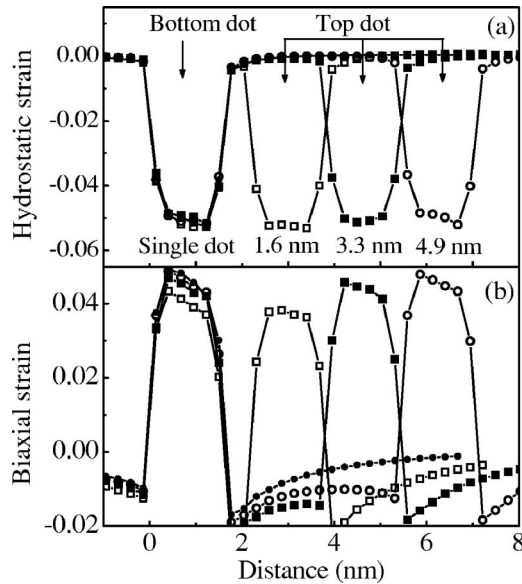
FIG. 14. (a) Hydrostatic and (b) biaxial components of the strain for the single-layer sample (filled circles) and double-dot structures as a function of the position from the bottom boundary of the bottom wetting layer along the z axis through the pyramidal apex. The dot spacing is $t_{Si} = 1.64$, 3.27, and 4.91 nm.

for the hole ground-state configuration to undergo such transformations is traced in the strain field distribution. It is seen in Fig. 14(b) that, for small t_{Si}, the biaxial strain field is different on both geometrically identical dots due to the lack of inversion symmetry with respect to the medium plane between the dots. The *top* Ge island *is less strained*. There are two effects which influence the formation of a molecule-type orbital in opposite way. The first one, characterized by the overlap integral Q, is the quantum-mechanical coupling between the individual states of two dots constituting the molecule. The second is the strain anisotropy which shifts the ground states of the dots far from resonance with one another yielding the difference of the original energy levels of the dots, ΔE. The molecular bond appears when

$$Q > \Delta E. \tag{12}$$

Both Q and ΔE vanish with increasing the interdot separation. For small distance ($t_{Si} < 3.3$ nm) the overlap integral is exponentially large implying strong coupling between the dots; for large separation ($t_{Si} > 3.8$ nm) the two dots do no longer feel each other through the superimposed strain fields and the energy difference ΔE goes to zero. In both cases the

condition (12) is fulfilled resulting in formation of a molecule-type hole state delocalized fairly over the two dots. For the intermediate distance (3.3 nm $\leqslant t_{Si} \leqslant 3.8$ nm), which is the characteristic length of strain decay in Si [see, Fig. 14(b)], the individual energy mismatch exceeds the overlap integral and the hole turns out to be confined inside the bottom, most strained Ge dot.

It is necessary to note that one-to-one comparison between theory and experiment (see, Fig. 13) is not quite appropriate here, because strain field superposition of buried Ge islands can cause enhanced Ge–Si material intermixing upon stacking of Ge dots.[40,91] As a result, the composition of double dot system may deviate from that of a single layer. At large gate voltage U_b, the strong electric field shifts the individual energy levels of the two dots far from resonance with one another, and the hole state becomes localized in the bottom dot. Because the Ge content in QDs is somewhat reduced in the stacked structures, the individual hole energy levels of a double-dot system are expected to be more shallow than that of a single dot. It is very likely that this effect is responsible for crossing of the hole states for single- and double-layer samples with $t_{Si} = 2$ and 2.5 nm observed for small filling factor (i.e., large gate voltage) in Fig. 12.

Furthermore, the Si content in the Si spacer layer can be decreased due to interdiffusion of Ge into Si leading to formation of a Ge-rich alloy in the coupling region between the dots.[92] The phenomenon of SiGe alloying in the Si barrier would reduce the effective tunneling distance for holes thereby enlarging the overlap integral Q. Probably this is origin of the difference between the calculated and measured energies observed in Fig. 13 at smallest t_{Si}, where the effect of Ge–Si alloying on the wave function overlapping is expected to be most pronounced. Nonetheless, the overall agreement between theory and experiment is quite good, indicating the crucial role played by strain fields in formation of hole states of self-assembled Ge/Si quantum-dot molecules.

VI. SUMMARY

Using the admittance spectroscopy, we have studied the single-particle ground state of a hole in two vertically coupled Ge quantum dots in Si. For a dot separation larger than 3 nm the hole binding energy in double dots was observed to be smaller than the ionization energy of single dot. The interpretation of our experimental results is based on the
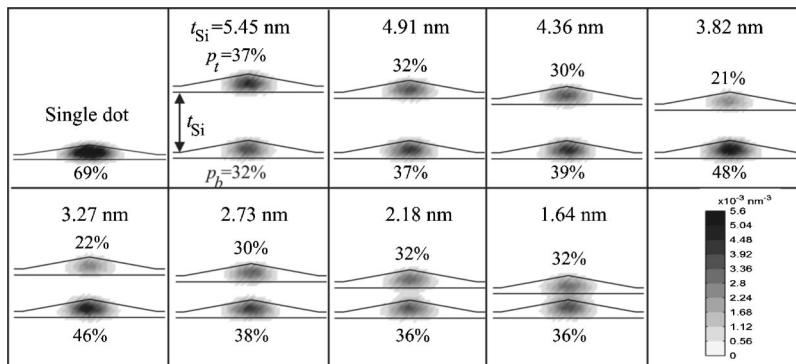

FIG. 15. The probability density of the ground hole state across the y-z plane of symmetry, cutting through the pyramids and the wetting layers. The probability to find the hole inside the bottom (p_b) or the top dot (p_t) is shown near each structure. Note that the quantity $p_b + p_t$ is not equal to 100% because a part of the hole state resides in the Si barrier.

application of sp^3 tight-binding approach in combination with the valence-force-field model. Both quantum-mechanical tunneling and inhomogeneous strain distribution due to the lattice mismatch between Ge and Si were included. For small and large interdot distances formation of covalentlike molecular orbital is recovered. We found that anomalous decreasing of the hole binding energy below the value of the single dot with increasing interdot separation is caused by the partial strain relaxation upon dot stacking accompanied by the strain-induced reduction of the hole confinement potential. For intermediate distances, where the difference of the original energy levels of the two dots exceeds the overlap integral, the localization of hole inside the bottom Ge dot is predicted.

ACKNOWLEDGMENTS

[1] A. Barenco, D. Deutsch, A. Ekert, and R. Jozsa, Phys. Rev. Lett. **74**, 4083 (1995).

[2] P. Zanardi and F. Rossi, Phys. Rev. Lett. **81**, 4752 (1998).

[3] D. Loss and D. P. DiVincenzo, Phys. Rev. A **57**, 120 (1998).

[4] E. Biolatti, R. C. Iotti, P. Zanardi, and F. Rossi, Phys. Rev. Lett. **85**, 5647 (2000).

[5] X.-Q. Li and Y. Arakawa, Phys. Rev. A **63**, 012302 (2000).

[6] M. Bayer, P. Hawrylak, K. Hinzer, S. Fafard, M. Korkunski, Z. R. Wasilewskii, O. Stern, and A. Forchet, Science **291**, 451 (2001).

[7] F. R. Waugh, M. J. Berry, D. J. Mar, R. M. Westervelt, K. L. Campman, and A. C. Gossard, Phys. Rev. Lett. **75**, 705 (1995).

[8] T. Hatano, M. Stopa, and S. Tarucha, Science **309**, 268 (2005).

[9] R. M. Abolfath and P. Hawrylak, Phys. Rev. Lett. **97**, 186802 (2006).

[10] For a review, see W. G. van der Wiel, S. De Franceschi, J. M. Elzerman, T. Fujisawa, S. Tarucha, and L. P. Kouwenhoven, Rev. Mod. Phys. **75**, 1 (2003).

[11] T. Schmidt, R. H. Haug, K. v. Klitzing, A. Förster, and H. Lüth, Phys. Rev. Lett. **78**, 1544 (1997).

[12] S. Amaha, D. G. Austing, Y. Tokura, K. Muraki, K. Oho, and S. Tarucha, Solid State Commun. **119**, 183 (2001).

[13] M. Pi, A. Emperador, M. Barranco, F. Garcias, K. Muraki, S. Tarucha, and D. G. Austing, Phys. Rev. Lett. **87**, 066801 (2001).

[14] D. S. Gandolfo, D. A. Williams, and H. Qin, J. Appl. Phys. **97**, 063710 (2005).

[15] J. Tersoff, C. Teichert, and M. G. Lagally, Phys. Rev. Lett. **76**, 1675 (1996).

[16] L. R. C. Fonseca, J. L. Jimenez, and J. P. Leburton, Phys. Rev. B **58**, 9955 (1998).

[17] C. Pryor, Phys. Rev. Lett. **80**, 3579 (1998).

[18] M. Korkusinski and P. Hawrylak, Phys. Rev. B **63**, 195311 (2001).

[19] W. Sheng and J.-P. Leburton, Phys. Rev. Lett. **88**, 167401 (2002).

[20] L. He, G. Bester, and A. Zunger, Phys. Rev. B **72**, 081311 (2005); **72**, 195307 (2005).

[21] R. J. Luyken, A. Lorke, M. Fricke, J. P. Kotthaus, G. Medeiros-Ribeiro, and P. M. Petroff, Nanotechnology **10**, 14 (1999).

[22] P. Boucaud, J. B. Williams, K. S. Gill, M. S. Sherwin, W. V. Schoenfeld, and P. M. Petroff, Appl. Phys. Lett. **77**, 4356 (2000).

[23] I. Shtrichman, C. Metzner, B. D. Gerardot, W. V. Schoenfeld, and P. M. Petroff, Phys. Rev. B **65**, 081303 (2002).

[24] A. M. Adawi, E. A. Zibik, L. R. Wilson, Al. Lemaître, W. D. Sheng, J. W. Cockburn, M. S. Skolnick, L. P. Leburton, M. Hopkinson, G. Hill, S. L. Liew, and A. G. Cullis, Phys. Status Solidi B **238**, 341 (2003).

[25] T. Bryllert, M. Borgstrom, L.-E. Wernersson, W. Siefert, and L. Samuelson, Appl. Phys. Lett. **82**, 2655 (2003).

[26] T. Ota, K. Ono, M. Stopa, T. Hatano, S. Tarucha, H. Z. Song, Y. Nakata, T. Miyazawa, T. Ohshima, and N. Yokoyama, Phys. Rev. Lett. **93**, 066801 (2004).

[27] M. M. Sobolev, G. E. Zirlin, Yu. B. Samsonenko, N. K. Polyakov, A. A. Tonkikh, and Yu. G. Musikhin, Semiconductors **39**, 119 (2005).

[28] A. I. Yakimov, A. V. Dvurechenskii, A. I. Nikiforov, and O. P. Pchelyakov, Thin Solid Films **336**, 332 (1998).

[29] F. Yuan, Z. Jiang, and F. Lu, Appl. Phys. Lett. **89**, 072112 (2006).

[30] For review, see I. Berbezier, A. Ronda, and A. Portavoce, J. Phys.: Condens. Matter **14**, 8283 (2002); C. Teichert, Phys. Rep. **365**, 335 (2002); K. Brunner, Rep. Prog. Phys. **65**, 27 (2002); J. Stangl, V. Holý, and G. Bauer, Rev. Mod. Phys. **76**, 725 (2004); J.-M. Baribeau, X. Wu, N. L. Rowel, and D. J. Lockwood, J. Phys.: Condens. Matter **18**, R139 (2006); A. I. Yakimov, A. V. Dvurechenskii, and A. I. Nikiforov, in *Handbook of Semiconductor Nanostructures and Nanodevices*, edited by A. A. Balandin and K. L. Wang (American Scientific, New York, 2006), Vol. 1, p. 33.

[31] Localization of electronic states in Ge/Si QDs is possible due to inhomogeneous tensile strain in Si around the buried Ge dots in multilayer Ge/Si structures. See, e.g, A. I. Yakimov, A. I. Nikiforov, and A. V. Dvurechenskii, Appl. Phys. Lett. **89**, 163126 (2006), and references therein.

[32] G. L. Bir and G. E. Pikus, *Symmetry and Strain-Induced Effects in Semiconductors* (Wiley, New York, 1974).

[33] C. G. Van de Walle, Phys. Rev. B **39**, 1871 (1989).

[34] A. V. Nenashev, A. V. Dvurechenskii, and A. F. Zinovieva, Phys. Rev. B **67**, 205301 (2003).

[35] P. Sutter and M. G. Lagally, Phys. Rev. Lett. **81**, 3471 (1998).

[36] A. Rastelli, E. Müller, and H. von Känel, Appl. Phys. Lett. **80**, 1438 (2002).

[37] Y. Q. Wu, F. H. Li, J. Cui, J. H. Lin, R. Wu, J. Qin, C. Y. Zhu, Y. L. Fan, X. J. Yang, and Z. M. Jiang, Appl. Phys. Lett. **87**, 223116 (2005).

[38] M. De Seta, G. Capellini, L. Di Gaspare, F. Evangelisti, and F. D'Acapito, J. Appl. Phys. **100**, 093516 (2006).

[39] A. I. Yakimov, A. I. Nikiforov, A. V. Dvurechenskii, V. V. Ulyanov, V. A. Volodin, and R. Groetzschel, Nanotechnology **17**, 4743 (2006).

[40] O. G. Schmidt, U. Denker, S. Christiansen, and F. Ernst, Appl. Phys. Lett. **81**, 2614 (2002).

[41] A. J. Kubis, T. E. Vandervelde, J. C. Bean, D. N. Dunn, and R. Hull, Appl. Phys. Lett. **88**, 263103 (2006).

[42] Y.-W. Mo, D. E. Savage, B. S. Swartzentruber, and M. G. Lagally, Phys. Rev. Lett. **65**, 1020 (1990).

[43] W.-H. Chang, W. Y. Chen, M. C. Cheng, C. Y. Lai, T. M. Hsu, N.-T. Yeh, and J.-I. Chyi, Phys. Rev. B **64**, 125315 (2001).

[44] W.-H. Chang, W. Y. Chen, T. M. Hsu, N.-T. Yeh, and J.-I. Chyi, Phys. Rev. B **66**, 195337 (2002).

[45] C. M. A. Kapteyn, F. Heinrichsdorff, O. Stier, R. Heitz, M. Grundmann, N. D. Zakharov, D. Bimberg, and P. Werner, Phys. Rev. B **60**, 14265 (1999).

[46] C. M. A. Kapteyn, M. Lion, R. Heitz, D. Bimberg, P. N. Brunkov, B. V. Volovik, S. G. Konnikov, A. R. Kovsh, and V. M. Ustinov, Appl. Phys. Lett. **76**, 1573 (2000).

[47] S. Schulz, S. Schnüll, Ch. Heyn, and W. Hansen, Phys. Rev. B **69**, 195317 (2004).

[48] M. Geller, A. Marent, E. Stock, D. Bimberg, V. I. Zubkov, I. S. Shulganova, and A. V. Solomonov, Appl. Phys. Lett. **89**, 232105 (2006).

[49] S. K. Zhang, H. J. Zhu, F. Lu, Z. M. Jiang, and X. Wang, Phys. Rev. Lett. **80**, 3340 (1998).

[50] C. M. A. Kapteyn, M. Lion, R. Heitz, D. Bimberg, C. Miesner, T. Asperger, K. Brunner, and G. Absreiter, Appl. Phys. Lett. **77**, 4169 (2000).

[51] C. Miesner, T. Asperger, K. Brunner, and G. Abstreiter, Appl. Phys. Lett. **77**, 2704 (2000).

[52] A. V. Dvurechenskii, A. V. Nenashev, and A. I. Yakimov, Nanotechnology **13**, 75 (2002).

[53] H. Zhou, S. Huang, Y. Rao, Z. Jiang, and F. Lu, Solid State Commun. **125**, 161 (2003).

[54] A. I. Yakimov, A. V. Dvurechenskii, V. A. Volodin, M. D. Efremov, A. I. Nikiforov, G. Yu. Mikhalyov, E. I. Gatskevich, and G. D. Ivlev, Phys. Rev. B **72**, 115318 (2005).

[55] G. Vincent, A. Chantre, and D. Bois, J. Appl. Phys. **50**, 5484 (1979).

[56] K. Schmalz, I. N. Yassievich, P. Schittenhelm, and G. Abstreiter, Phys. Rev. B **60**, 1792 (1999).

[57] S. Anand, N. Carlsson, M.-E. Pistol, L. Samuelson, and W. Seifert, J.

Appl. Phys. **84**, 3747 (1998).

[58]H. Kroemer, W.-Y. Chien, J. S. Harris, Jr., and D. D. Edwall, Appl. Phys. Lett. **36**, 295 (1980).

[59]V. Ya. Aleshkin, N. A. Bekin, M. N. Buyanova, A. V. Murel, and B. N. Zvonkov, Semiconductors **33**, 1133 (1999).

[60]S. M. Sze, *Physics of Semiconductor Devices* (Wiley, New York, 1981), Vol. 1.

[61]We point out that the final result, i. e., the $\nu(U_b)$ data, does not dependend on the exact choice of U_{b0}. It is only essential that QDs would be neutral at U_{b0}.

[62]P. N. Keating, Phys. Rev. **145**, 637 (1966).

[63]R. Martin, Phys. Rev. B **1**, 4005 (1970).

[64]M. A. Cusack, P. R. Briddon, and M. Jaros, Phys. Rev. B **54**, R2300 (1996).

[65]C. Pryor, J. Kim, L. W. Wang, A. J. Williamson, and A. Zunger, J. Appl. Phys. **83**, 2548 (1998).

[66]L. W. Wang, J. Kim, and A. Zunger, Phys. Rev. B **59**, 5678 (1999).

[67]A. V. Nenashev and A. V. Dvurechenskii, JETP **91**, 497 (2000).

[68]A. J. Williamson, L. W. Wang, and A. Zunger, Phys. Rev. B **62**, 12963 (2000).

[69]Y. Kikuchi, H. Sugii, and K. Shintani, J. Appl. Phys. **89**, 1191 (2001).

[70]J. H. Seok and J. Y. Kim, Appl. Phys. Lett. **78**, 3124 (2001); J. Y. Kim and J. H. Seok, Mater. Sci. Eng., B **89**, 176 (2002).

[71]M. El Kurdi, S. Sauvage, G. Fishman, and P. Boucaud, Phys. Rev. B **73**, 195327 (2006).

[72]A. I. Yakimov, A. V. Dvurechenskii, A. I. Nikiforov, A. A. Bloshkin, A. V. Nenashev, and V. A. Volodin, Phys. Rev. B **73**, 115333 (2006).

[73]A. I. Yakimov, G. Yu. Mikhalyov, A. V. Nenashev, and A. V. Dvurechenskii, JETP Lett. **85**, 429 (2007).

[74]M. Grundmann, O. Stier, and D. Bimberg, Phys. Rev. B **52**, 11969 (1995).

[75]T. Benabbas, P. Francois, Y. Androussi, and A. Lefebvre, J. Appl. Phys. **80**, 2763 (1996).

[76]T. Benabbas, Y. Androussi, and A. Lefebvre, J. Appl. Phys. **86**, 1945 (1999).

[77]O. G. Schmidt, K. Eberl, and Y. Rau, Phys. Rev. B **62**, 16715 (2000).

[78]T. Saito, T. Nakaoka, T. Katitsuka, Y. Yoshikuni, and Y. Arakawa, Physica E (Amsterdam) **26**, 217 (2005).

[79]J. C. Slater and G. F. Koster, Phys. Rev. **94**, 1498 (1954).

[80]D. J. Chadi and M. L. Cohen, Phys. Status Solidi B **68**, 405 (1975).

[81]D. J. Chadi, Phys. Rev. B **16**, 790 (1977).

[82]F. B. Pedersen and Y.-C. Chang, Phys. Rev. B **53**, 1507 (1996).

[83]P. N. Brounkov, S. G. Konnikov, V. M. Ustinov, A. E. Zhukov, A. Yu. Egorov, M. Maximov, N. N. Ledentsov, and P. S. Kop'ev, Semiconductors **30**, 492 (1996); P. N. Brounkov, A. Polimeni, S. T. Stoddart, M. Henini, L. Eaves, P. C. Main, A. R. Kovsh, Yu. G. Musikhin, and S. G. Konnikov, Appl. Phys. Lett. **73**, 1092 (1998).

[84]H. L. Wang, F. H. Yang, S. L. Feng, H. J. Zhu, D. Ning, H. Wang, and X. D. Wang, Phys. Rev. B **61**, 5530 (2000).

[85]M. Geller, C. Kapteyn, L. Müller-Kirsch, R. Heitz, and D. Bimberg, Appl. Phys. Lett. **82**, 2706 (2003).

[86]P. M. Mooney, L. J. Cheng, M. Süli, J. D. Gerson, and J. W. Corbett, Phys. Rev. B **15**, 3836 (1977).

[87]V. Higgs, P. Kightley, P. J. Goodhew, and P. D. Augustus, Appl. Phys. Lett. **59**, 829 (1991); S. Fukatsu, Y. Mera, M. Inoue, K. Maeda, H. Akiyama, and H. Sakaki, *ibid.* **68**, 1889 (1996); O. G. Schmidt, U. Denker, K. Eberl, O. Kienze, and F. Ernst, *ibid.* **77**, 2509 (2000); K. E. Sun, S. H. Sue, and C. W. Liu, Physica E (Amsterdam) **28**, 525 (2005); C. M. Wei, T. T. Chen, Y. F. Chen, Y. H. Peng, and C. H. Kuan, Appl. Phys. Lett. **90**, 061912 (2007).

[88]J. Zhang and B. I. Shklovskii, Phys. Rev. B **70**, 115317 (2004).

[89]F. H. Pollak and M. Cardona, Phys. Rev. **172**, 816 (1968).

[90]M. Califano and P. Harrison, J. Appl. Phys. **91**, 389 (2002).

[91]O. G. Schmidt and K. Eberl, Phys. Rev. B **61**, 13721 (2000).

[92]M. Meduňa, J. Novák, G. Bauer, V. Holý, C. V. Falub, S. Tsujino, and D. Grützmacher, Semicond. Sci. Technol. **22**, 447 (2007).